Case Studies in Thermal Engineering 24 (2021) 100861

Contents lists available at ScienceDirect

Case Studies in Thermal Engineering

journal homepage: http://www.elsevier.com/locate/csite

Energy conservation of nanofluids from a biomagnetic needle in the presence of Stefan blowing: Lie symmetry and numerical simulation

O. Anwar Beg [a], F.T. Zohra [b,c], M.J. Uddin [b,c], A.I.M. Ismail [b], Saratha Sathasivam [b,*]

[a] Multiphysical Engineering Sciences Group, SEE, Salford University, Manchester, M54WT, UK
[b] School of Mathematical Sciences, Universiti Sains Malaysia, 11800, USM, Penang, Malaysia
[c] Mathematics Department, American International University- Bangladesh, Kuratoli, Dhaka, 1229, Bangladesh

ARTICLE INFO

Keywords:
Biomagnetic needle
Nano-bioconvection
Stefan blowing
Lie symmetry
Bvp5c

ABSTRACT

Thermal energy management associated with the transmission of heat is one of the main problems in many industrial setups (e.g. pharmaceutical, chemical and food) and bio-engineering devices (e.g. hospital ventilation, heating, cooling devices, heat exchanger and drying food, etc). The current study aims to examine thermo-bioconvection of oxytactic microorganisms taking place in a nanofluid-saturated needle with the magnetic field. Stefan-blowing is applied. The leading equations of continuity, momentum and energy, species transport equations for oxygen concentration and population density of microorganisms are reduced dimensionless and Lie symmetry group transformations are used to generate appropriate invariant transformations. The resulting similarity boundary value problem (in which the blowing parameter is coupled with concentration) have been simulated using **MATLAB** (2015a) bvp5c built in function. The impact of the emerging factors on the nondimensional velocity, temperature, nanoparticle concentration and motile microorganism density functions and their slopes at the wall, are pictured and tabulated. Justification with published results are included. It is found that all physical quantities decrease with Stefan blowing and increase with power law index parameter. With elevation in magnetic field parameter i.e., Lorentzian drag force, the friction factor reduces while the local Nusselt number, local Sherwood number, and the local motile microorganism density wall gradient increase. Present study could be used in food and pharmaceutical industries, chemical processing equipment, fuel cell technology, enhanced oil recovery, etc.

1. Introduction

Investigation of the hydrodynamics of electrically conducting liquids/gases subjected to a magnetic field is known as magneto-hydrodynamics (MHD). MHD phenomena have many industrial applications [1]. Recent trends in nanotechnology have witnessed a proliferation in deployment of *nanofluids*. A new sub-set of these nano-scaled engineered liquids are magnetic nanofluids which are synthesized via the careful suspension of magnetic nanoparticles within a base fluid e.g. air, lubricants, water, etc. Magnetic nanofluids provide a mechanism for controlling flow, heat/mass and microorganism transfer rates with the imposition of an exterior magnetic field which may be static or oscillatory. These characteristics of a magneto-nanofluids make them ideal for many complex applications

* Corresponding author.
E-mail address: saratha@usm.my (S. Sathasivam).

https://doi.org/10.1016/j.csite.2021.100861
Received 14 November 2020; Received in revised form 30 December 2020; Accepted 19 January 2021
Available online 28 January 2021

Nomenclature

$\widetilde{b}$	chemotaxis constant (m)
C	fluid concentration $(-)$
C_p	specific heat at constant pressure $\left(\frac{J}{Kg\,K}\right)$
C_w	needle surface concentration $(-)$
C_∞	free stream concentration $(-)$
$C_{f\,\bar{x}}$	local skin friction coefficient$(\ -\ )$
D_B	Brownian diffusion coefficient $\left(\frac{m^2}{s}\right)$
D_m	micro-organism diffusivity coefficient $\left(\frac{m^2}{s}\right)$
D_n	diffusivity coefficient $\left(\frac{m^2}{s}\right)$
D_T	thermophoretic diffusion coefficient $\left(\frac{m^2}{s}\right)$
$f(\eta)$	dimensionless stream function$(\ -\ )$
k_f	effective thermal conductivity of the fluid$\left(\frac{W}{m\cdot K}\right)$
k_s	effective thermal conductivity of the solid fraction $\left(\frac{W}{m\cdot K}\right)$
k_{nf}	effective thermal conductivity of the nanofluid $\left(\frac{W}{m\cdot K}\right)$
L	characteristic length (m)
Lb	Lewis number $(\ -\ )$
m	power law parameter $(\ -\ )$
M	magnetic parameter $(-)$
Nb	Brownian motion parameter $(\ -\ )$
$N_{n_{\bar{x}}}$	local density number of motile microorganisms$(\ -\ )$
Nt	thermophoresis parameter $\left(\frac{\tau D_T(T_w-T_\infty)}{\alpha T_\infty}\right)(\ -\ )$
$N_{u_{\bar{x}}}$	local Nusselt number $(\ -\ )$
n	number of motile micro-organisms$(\ -\ )$
n_w	number of motile micro-organisms at wall (wedge face)$(\ -\ )$
n_∞	ambient number of motile micro-organisms$(\ -\ )$
P	pressure$\left(\frac{kg}{m\,s^2}\right)(\ -\ )$
Pe	Péclet number $(\ -\ )$
Pr	Prandtl number$(\ -\ )$
Re	Reynolds number$(\ -\ )$
$Re_{\bar{x}}$	local Reynolds number$(\ -\ )$
s	blowing parameter $(\ -\ )$
Sb	bioconvection Schmidt number$(\ -\ )$
Sc	Schmidt number$(\ -\ )$
$Sh_{\bar{x}}$	local Sherwood number $(\ -\ )$
T	nanofluid temperature (K)
T_w	dimensional surface temperature at the wall(K)
T_∞	dimensional ambient temperature(K)
$\bar{u},\ \bar{v}$	dimensional velocity components along the $\bar{x}-$ and $\bar{r}-$ axes $\left(\frac{m}{s}\right)$
U_∞	reference velocity $\left(\frac{m}{s}\right)$
u, v	dimensionless velocity components along the $\bar{x}-$ and $y-$ axes$(\ -\ )$
W_c	maximum cell swimming speed $\left(\frac{m}{s}\right)$
$\bar{x}$, $\bar{r}$	coordinates along and normal to the needle (m)
x, r	dimensionless coordinates along and normal to the needle (m)

in which *smart control* is required including thermal engineering, surface treatment of aerospace materials, electromagnetic biomedical devices (pumps, surgical flow control, meters) etc [2–4]. To improve the performance of magneto-nanofluids, and as an important compliment to e.g. clinical and experimental testing, mathematical and numerical simulations are critical. This has motivated many researchers to investigate the dynamics of magnetic nanofluids both within and external to diverse geometrical configurations (plates, channels, cones, spheres, wavy tubes, curved surfaces etc) subject to various boundary conditions. MHD transport problems have therefore emerged as a main sub-set of modern nanofluid transport problems. Magnetic nanofluids have been studied feature many types of metallic nano-particle adjourned in dilute fluent media along with aluminium oxide, gold, silver, titanium, zinc, copper etc. Furthermore, a diverse spectrum of methods (analytical, semi-analytical/numerical, approximiation) have been used to simulate the nonlinear similarity and non-similarity problems characterizing magnetic nanofluid flows and such studies have also featured many supplementary multi-physical effects of relevance to medical engineering. Bég et al. [5] studied the hydromagnetic squeeze film dynamics of magneto-nanofluids using spectral collocation methods, noting that Brownian motion and nano-particle size have a profound influence on loading capacity, heat dissipation and velocity distributions. Hsiao [6] presented numerical finite difference solutions for micropolar magnetic nanofluids over stretchable sheet, observing that higher magnetic field reduces Nusselt number whereas it elevates shear stress, couple stress at the surface, temperature and concentration. López et al. [7] investigated generation of entropy in the presence of MHD flow of Al_2O_3–water nanofluid via a radiative microchannel numerically.

Bioconvection occurs if motile microorganisms responding to specific stimuli (e.g. such as light, the attraction of chemical agents, gravity, oxygen, etc.) swim with a directional bias in a pool of liquid. Depending on the stimuli (taxes), several types of bioconvection (phototactic, chemotactic, gravitactic, oxytactic, etc.) may occur. Normally, the self-propelled motile microorganisms are marginally denser than the liquid in which they move. It appeared as a substantial subdivision of modern fluid dynamics, mainly driven by auspicious uses in fuel cell and green energy technologies. Bioconvection refers to the occurrence of macroscopic convective flow produced by the density difference generated via collective swimming of microorganisms. Note that self-propelled microorganisms tend to gather at the vicinity of the top portion of fluid layer, which in-turn lead to heavier top than the bottom region [8]. Bioconvection features in numerous industrial and environmental (ecological) systems including pharmaceutics [9] and gas-bearing sedimentary bio-microsystems [10]. Laboratory and field experiments have shown that the introduction of micro-organisms in nanofluids results in a sustained superior thermal performances as well as green, sustainable characteristics. These developments are foundational for further progress in next generation biofuels. In the regions adjacent to the wall of bio-engineered devices, boundary layers play a critical role. Recent illustration of bioconvection include the project of bioethanol power sources [11], ecological fuel

Greek symbols

α	effective thermal diffusivity $\left(\frac{m^2}{s}\right)$
η	independent similarity variable $\left(\frac{m^2}{s}\right)$
μ	dynamic viscosity of the fluid $\left(\frac{kg}{m\,s}\right)$
μ_m	magnetic permeability $\left(\frac{kg\,m}{s^2A^2}\right)$
υ	kinematic viscosity of the fluid $\left(\frac{m^2}{s}\right)$
ρ	fluid density $\left(\frac{kg}{m^3}\right)$
ρ_f	density of the base fluid $\left(\frac{kg}{m^3}\right)$
$(\rho c_p)_{nf}$	heat capacitance of the nanofluid $\left(\frac{J}{m^3K}\right)$
$(\rho c)_f$	heat capacitance of the base fluid $\left(\frac{J}{m^3K}\right)$
$(\rho c)_p$	heat capacitance of the nanoparticles $\left(\frac{J}{m^3K}\right)$
σ_{nf}	electric conductivity of the nanofluid (Siemens/m)
τ	ratio of the effective heat capacity of the nanoparticle to the fluid heat capacity(−)
θ	dimensionless temperature (−)
Φ	nanoparticle volume fraction (−)
ϕ	dimensionless concentration (−)
χ	dimensionless number density of motile microorganisms(−)
ψ	dimensionless stream function (−)

Subscripts

$()'$	differentiation with respect to η

cells [12] and photo-bio-reactors [13,14].

Biomass can be obtained from microalgae in bioconvection by adjusting the flue gas condition and which yields in the synthesis of more effective photobioreactors [14]. It is important to note that in the same way that many types of nanofluid [15,16] may be fabricated with different nano-particles (metallic, carbon nanotubes, nano-wires, nano-shells), bioconvection also manifests in different types of micro-organisms. The micro-organisms are driven by a *taxis (stimulus)* which may be light (photo-tactic), magnetic field (magneto-tactic), oxygen (oxy-tactic), electrical field (electro-tactic) or hydrodynamic torque (gyro-tactic). These and other engineering applications have recently been reviewed by Sohail and Li [17]. The rich spectrum of nonlinear boundary value problems furnished by combined nanofluid bioconvection flows have stimulated considerable interest among engineering scientists in recent years and have featured extensive multi-physical aspect. Uddin et al. [18] have studied numerically the effects of blowing on nano-bio convection. Other investigations include MHD radiative nano-bioconvection flow [19], unsteady tribological squeeze nanofluid bioconvection [20], MHD bioconvection in two-phase dusty nanofluids [21], nano-bioconvection channel flow [22], peristaltic pumping of Sisko rheological bioconvection nanofluids in a curved channel [23], thermal aspects of Carreau fluid [24–26], Powell-Erying fluid [27], hyperbolic fluid [28] and axisymmetric swirl MHD flow with anisotropic slip and Stefan blowing from a rotating cone [29].

A thin needle is a slender body with the geometry having paraboloid of revolution. External flow past a needle is normally *axisymmetric*. Transport phenomena from a needle constitutes quite an active research topic in *biomedical engineering* where it arises in, for example, cancer therapy and dermal administration of drugs. It is also of significance in industrial processes e.g. in metal spinning and in micro/nano scale equipment [30] including the removal of subterranean nuclear waste [31]. Many features of flow with heat/mass transfer from needles with many wall conditions have been examined (both numerically and analytically) by many researchers. A seminal study was communicated over four decades ago by Narain and Uberoi [32]. They also observed that with a reduction in needle size (with constrained Prandtl and local Reynolds and Grashof number), there is an elevation in skin-friction coefficient and Nusselt number. Wang [33] explored mixed convective flow on a vertical slender adiabatic paraboloidal needle with a tip heat source, identifying that for positive values of heat source parameter (aiding flow) the solutions are unique whereas for negative heat source parameter (opposing flow) solutions may be unique, dual, or non-existent. Ishak et al. [34] examined the combined free and forced convective flow from a continuously moving needle. Trimbitas et al. [35] considered mixed convective nanofluid flow along thin needles for a Prandtl number of 6.2 and described in detail the influence of nano-particle solid volume fraction on thermal/flow characteristics. Hayat et al. [36] used a shooting numerical method to obtain comprehensive solutions for water-based carbon nanofluid flow with variable heat flux along a thin needle, noting that significant flow acceleration is induced with increasing nanoparticle volume fraction. Sulochana et al. [37] studied magneto-convective radiative forced nanofluid with Joule heating along a continuously moving horizontal needle for the cases of Al50Cu50 (alloy with 50% alumina and 50% copper)-water and Copper-water nanofluid using the Tiwari-Das volume fraction model. The effect of the shape of the nanoparticles, thermophoresis and Brownian moment in a lopsided needle are discussed by Akbar et al. [38,39]. They also discussed the analytic approach of heat transfer for CNT nanofluid through a ciliated porus medium [40], ferromagnetic peristaltic flow in a plumb duct [41] and micropolar biological flow due to metachronal wave [42]. Ahmad et al. [43] illustrated nanofluid flow from a thin needle using the bvp4c quadrature routine, showing that needle velocity assists in wall shear stress enhancement and heat transfer rate is increased with decreasing thermophoresis. Afridi and Qasim [44] conducted a second law thermodynamic analysis of boundary layer radiative-convective flow over a thin needle moving in a parallel stream.

The majority of thermo-fluid dynamics studies of external boundary layer flows from a needle have been restricted to the solid wall case and have generally considered heat/mass transfer along either isothermal/non-isothermal or constant/variable wall heat flux needles. The present paper extends these studies to consider *gyrotactic micro-organism bioconvection in forced convective magneto-nanofluid flow from a needle with Stefan blowing (suction/injection coupled with the concentration)*. Similarity equations for the transport problem are derived with the aid of stretching group transformations. The Tiwari-Das model [45] is employed for nanoparticle

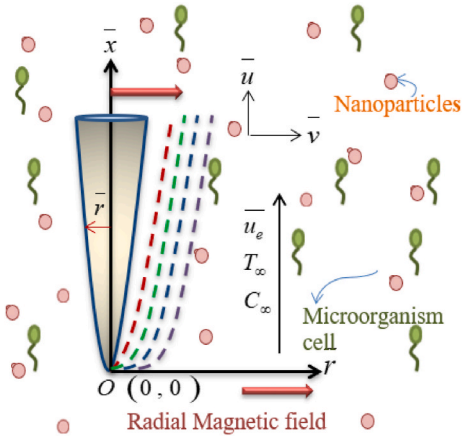

Fig. 1. Flow model and coordinates system.

volume fraction and studying different metals and metallic oxides in water. The normalized nonlinear boundary value problem is numerically solved using the robust Matlab bvp5c symbolic software. Bvp5c is a finite difference code that solves multipoint boundary value problem by implementing four-stage Lobatto IIIa formula [46]. This is a collocation formula and the collocation polynomial provides a C [1]-continuous solution that is fifth-order accurate uniformly in interval [a,b]. The formula is implemented as an implicit Runge-Kutta formula. It solves the algebraic equations directly by augmenting the system with trivial differential equations for the unknown parameters and directly controls the true error in the calculation.

The present work considers several novel aspects which may be summarized as follows*: i) bio-convection in 4 different nanofluids (Cu*-water, Al_2O_3-water, *CuO*-water and TiO_2-water nanofluids*) is studied ii) the needle is porous and Stefan blowing is considered, iii) stretching group transformations are used to generate the similarity transformations, iv) magnetohydrodynamics is studied since the nanofluids are electrically-conducting and biomagnetic therapy utilizes such features.* Extensive computational results are presented for the impact of a variety of the thermo-physical parameters on flow, heat, mass and microorganism characteristics. Verification of the MATLAB solutions with published results also presented.

2. Thin needle magnetic nanofluid bioconvection model

2-D steady, axisymmetric forced convective viscous incompressible nanofluid flow containing micro-organisms in the region external to a vertical thin needle is considered. Flow model and system of coordinates is depicted in Fig. 1. External velocity is considered to change according to$(\overline{x}/L)^m$. A variable magnetic field $B(\overline{x}/L)$is used in the radial direction. The free stream nanofluid is at a constant temperature T_∞ and concentrationC_∞, while the needle wall temperature $T_w(\overline{x}/L)$, concentration$C_w(\overline{x}/L)$and micro-organism species density $n_w(\overline{x}/L)$ are varies with position x. The nanoparticles are assumed to dilute dispersed and do not change swimming direction and velocity of the micro-organisms. It is assumed that $\overline{r} = \overline{R}(\overline{x})$. The appropriate dimensionless equations in cylindrical coordinates are [32,45,47]:

$$\frac{1}{r^2}\frac{\partial \psi}{\partial r}\frac{\partial^2 \psi}{\partial r^2}+\frac{1}{r^3}\frac{\partial \psi}{\partial x}\frac{\partial \psi}{\partial r}-\frac{1}{r^2}\frac{\partial^2 \psi}{\partial r^2}\frac{\partial \psi}{\partial x}+\frac{\sigma_{nf}}{\rho_{nf}}\frac{L}{U_\infty}B^2(x)\frac{1}{r}\frac{\partial \psi}{\partial r}= u_e\frac{d\,u_e}{d\,x}+A_0\left(\frac{1}{r}\frac{\partial^3 \psi}{\partial r^3}-\frac{1}{r^2}\frac{\partial^2 \psi}{\partial r^2}+\frac{1}{r^3}\frac{\partial \psi}{\partial r}\right), \tag{1}$$

$$\frac{1}{r}\frac{\partial \psi}{\partial r}\frac{\partial \widetilde{\theta}}{\partial x}-\frac{1}{r}\frac{\partial \psi}{\partial x}\frac{\partial \widetilde{\theta}}{\partial r}=\frac{A_2}{\mathrm{Pr}}\left(\frac{1}{r}\frac{\partial \widetilde{\theta}}{\partial r}+\frac{\partial^2 \widetilde{\theta}}{\partial r^2}\right), \tag{2}$$

$$\frac{1}{r}\frac{\partial \psi}{\partial r}\frac{\partial \widetilde{\varphi}}{\partial x}-\frac{1}{r}\frac{\partial \psi}{\partial x}\frac{\partial \widetilde{\varphi}}{\partial r}=\frac{1}{\mathrm{Sc}}\left(\frac{1}{r}\frac{\partial \widetilde{\varphi}}{\partial r}+\frac{\partial^2 \widetilde{\varphi}}{\partial r^2}\right), \tag{3}$$

$$\frac{1}{r}\frac{\partial \psi}{\partial r}\frac{\partial \widetilde{\chi}}{\partial x}-\frac{1}{r}\frac{\partial \psi}{\partial x}\frac{\partial \widetilde{\chi}}{\partial r}+\frac{Pe}{Sb}\frac{\partial}{\partial r}\left(\frac{\partial \widetilde{\chi}}{\partial r}\frac{\partial \widetilde{\varphi}}{\partial x}+\widetilde{\chi}\frac{\partial^2 \widetilde{\varphi}}{\partial x^2}\right)\frac{1}{x^{2m-1}}=\frac{1}{\mathrm{Sb}}\left(\frac{1}{r}\frac{\partial \widetilde{\chi}}{\partial r}+\frac{\partial^2 \widetilde{\chi}}{\partial r^2}\right), \tag{4}$$

The boundary conditions are:

$$\frac{\partial \psi}{\partial r}=0,\ \frac{1}{r}\frac{\partial \psi}{\partial x}=\frac{s}{Sc\,x^{m-1}}\left(\frac{\partial C}{\partial r}\right),\ T=x^{2m-1},\ C=x^{2m-1}\ \text{ at }\ r=R(x), \tag{5}$$

$$\frac{1}{r}\frac{\partial \psi}{\partial r}=u_e(x)=x^m,\ T\to 0, C\ \to\ 0 \text{ as } r\to\infty, \tag{6}$$

Following variables were used for nondimensionalizing:

$$x=\frac{\overline{x}}{L},\ r=\frac{\overline{r}}{L}\sqrt{\mathrm{Re}},\ R(x)=\frac{\overline{R}(\overline{x})}{L}\sqrt{\mathrm{Re}}, u=\frac{\overline{u}}{U_\infty}, v=\frac{\overline{v}}{U_\infty}\sqrt{\mathrm{Re}}, u_e(x)=\frac{\overline{u}_e(\overline{x})}{U_\infty}, \widetilde{\chi}=\frac{n}{n_w},$$
$$\widetilde{\theta}=\frac{T-T_\infty}{T_w-T_\infty}, \widetilde{\varphi}=\frac{C-C_\infty}{C_w-C_\infty}, B^2(x)=B_0^2x^{m-1}, M^2=\frac{\sigma_f B_0^2 L}{U_\infty \rho_f}, ru=\frac{\partial \psi}{\partial r}, rv=-\frac{\partial \psi}{\partial x} \tag{7}$$

The properties of nanofluid may be computed, following [48–50] with the following relations which are all functions of the nano-particle solid volume fraction (Φ):

$$\mu_{nf}=\frac{\mu_f}{(1-\Phi)^{2.5}},\quad \rho_{nf}=(1-\Phi)\rho_f+\Phi\rho_s,\quad \upsilon_{nf}=\frac{\mu_{nf}}{\rho_{nf}}=\frac{\mu_f}{(1-\Phi)^{2.5}\left[(1-\Phi)\rho_f+\Phi\rho_s\right]},$$

$$\frac{\sigma_{nf}}{\sigma_f}=1+\frac{3\Phi\left(\frac{\sigma_s}{\sigma_f}-1\right)}{\left(\frac{\sigma_s}{\sigma_f}+2\right)-\Phi\left(\frac{\sigma_s}{\sigma_f}-1\right)},\quad \left(\rho C_p\right)_{nf}=(1-\Phi)\left(\rho C_p\right)_f+\Phi\left(\rho C_p\right)_s, \tag{8}$$

$$\alpha_{nf}=\frac{k_{nf}}{\left(\rho C_p\right)_{nf}},\quad \frac{k_{nf}}{k_f}=\frac{\left(k_s+2k_f\right)-2\Phi\left(k_f-2k_s\right)}{\left(k_s+2k_f\right)+\Phi\left(k_f-2k_s\right)}.$$

3. Derivation of similarity solutions

Obtaining analytical solutions of equations (1)–(6) are challenging even with numerical methods. So, it suitable to reduce them into relevant invariant equations. This is accomplished by deploying the following powerful stretching transformations [51,52]:

$$x=\alpha_1 x^*,\ r=\alpha_2 r^*,\ \psi=\alpha_3\psi^*,\ \widetilde{\theta}=\alpha_4\widetilde{\theta}^*,\ \widetilde{\varphi}=\alpha_5\widetilde{\varphi}^*,\ \widetilde{\chi}=\alpha_6\widetilde{\chi}^*, \tag{9}$$

Here α_i denotes the arbitrary real positive numbers for which the inter-relationship is required to be obtained at different $i=1,2,\ldots,6$. Eqns. (1)–(5) with boundary conditions in Eqn. (6) must remain *invariant* under the stretching transformations defined in Eqn. (9). After some simple algebraic manipulation, it may be shown that the governing Eqns. (1)–(6) will be invariant provided the following conditions are enforced:

$$\alpha_2=\alpha_1^{\frac{1-m}{2}},\ \alpha_3=\alpha_2,\quad \alpha_4=\alpha_5=\alpha_6=\alpha_2^{2m-1}. \tag{10}$$

Using (10), Eqn. (9) can be simplified to:

$$x=\alpha_1 x^*, r=\alpha_1^{\frac{1-m}{2}} r^*\ ,\ \psi=\alpha_1\psi^*,\ \widetilde{\theta}=\alpha_1^{2m-1}\widetilde{\theta}^*,\ \widetilde{\varphi}=\alpha_1^{2m-1}\widetilde{\varphi}^*,\ \widetilde{\chi}=\alpha_1^{2m-1}\widetilde{\chi}^*. \tag{11}$$

Eqn. (11) demonstrations that the PDEs (1–5) with boundary conditions (6) are free from α_1 under arrangements of the variables given below:

$$\frac{r^2}{x^{1-m}},\ \frac{\psi}{x},\ \frac{\widetilde{\theta}}{x^{2m-1}}\ ,\ \frac{\widetilde{\varphi}}{x^{2m-1}},\frac{\widetilde{\chi}}{x^{2m-1}}. \tag{12}$$

Hence the relevant invariant variable $\eta$and the functional forms for ψ, $\widetilde{\theta}$, $\widetilde{\varphi}$ and $\widetilde{\chi}$ can then be written as:

$$\eta=\frac{r^2}{x^{1-m}},\ \frac{\psi}{x}=f(\eta),\ \ \theta(\eta)=\frac{\widetilde{\theta}}{x^{2m-1}},\ \varphi(\eta)=\frac{\widetilde{\varphi}}{x^{2m-1}},\chi(\eta)=\frac{\widetilde{\chi}}{x^{2m-1}}. \tag{13}$$

Following ref [32], setting $\eta=a$, the relationship, $\eta=\frac{r^2}{x^{1-m}}$ describes *both the shape and the size of the body* considered with its surface assumed by:

$$R(x)=a^{1/2}x^{(1-m)/2}. \tag{14}$$

From Eq. (14) it can be seen that, for *pointed bodies and cylindersm* ≤ 1, $m=1$corresponds to a cylinder, $m=0$ corresponds to a paraboloid (blunt nosed configuration) and $m=-1$ corresponds to a cone. The parlance is, in fact, similar to that employed in hypersonic aerodynamic design [9].

Using Eqn. (13) into Eqns. (1)–(6), generates the following system of "self-similar "coupled, nonlinear equations:

$$8A_0(\eta f'''+f'')+4f''f-4m(f')^2+m-2A_1M^2f'=0 \tag{15}$$

$$\frac{2A_2}{\mathrm{Pr}}(\eta\theta''+\theta')+f\theta'-(2m-1)f'\theta=0 \tag{16}$$

$$\frac{2}{Sc}(\eta\varphi''+\varphi')+f\varphi'-(2m-1)f'\varphi=0 \tag{17}$$

$$\frac{2}{Sb}(\eta\chi''+\chi')+f\chi'-\frac{Pe}{Sb}(2\eta\chi'\varphi'+2\eta\chi\varphi''+\chi\varphi')-(2m-1)f'\chi=0 \tag{18}$$

The boundary conditions become:

$$f'(a)=0,\quad f(a)=\frac{2s}{Sc}a\varphi'(a),\quad \theta(a)=1,\quad \varphi(a)=1,\quad \chi(a)=1 \tag{19}$$

$$f'(+\infty)\to\frac{1}{2},\quad \theta(+\infty)\to 0,\quad \varphi(+\infty)\to 0,\quad \chi(+\infty)\to 0 \tag{20}$$

Note that the primes indicate *differentiation* with respect to η. In equations 15–20 the constants A_i $(i = 0, 1, 2)$ are defined as follows:

$$A_0 = \frac{1}{(1-\Phi)^{2.5}\left[1-\Phi+\Phi\frac{\rho_s}{\rho_f}\right]},$$

$$A_1 = \frac{\left[1+\frac{3\Phi\left(\frac{\sigma_s}{\sigma_f}-1\right)}{\left(\frac{\sigma_s}{\sigma_f}+2\right)-\Phi\left(\frac{\sigma_s}{\sigma_f}-1\right)}\right]}{1-\Phi+\Phi\frac{\rho_s}{\rho_f}},$$

$$A_2 = \frac{k_{nf}/k_f}{1-\Phi+\Phi\frac{(\rho C_p)_s}{(\rho C_p)_f}}.$$

$$A_1 = \frac{\left[1+\frac{3\Phi\left(\frac{\sigma_s}{\sigma_f}-1\right)}{\left(\frac{\sigma_s}{\sigma_f}+2\right)-\Phi\left(\frac{\sigma_s}{\sigma_f}-1\right)}\right]}{1-\Phi+\Phi\frac{\rho_s}{\rho_f}}, \tag{21}$$

It needs to mention that for regular fluid (no nanoparticles and micro-organism), in the absence of body force term for an isothermal needle (i.e. $m = 0.5$), the present model resembles to the model of Narain and Uberoi [32]. This further verifies the correctness of the group analysis presented earlier.

4. Engineering design quantities

Quanties of engineering interest (*local skin friction, the local Nusselt number, local Sherwood number and the local wall motile micro-organism number) are* defined as:

$$\mathrm{Re}_{\bar{r}}^{1/2} Cf_{\bar{x}} = \frac{4a^{1/2}}{(1-\Phi)^{2.5}} f''(a), \quad \mathrm{Re}_{\bar{x}}^{-1/2} Nu_{\bar{x}} = -\frac{k_{nf}}{k_f} 2a^{1/2}\theta'(a),$$
$$\mathrm{Re}_{\bar{x}}^{-1/2} Sh_{\bar{x}} = -2a^{1/2}\varphi'(a), \quad \mathrm{Re}_{\bar{x}}^{-1/2} Nn_{\bar{x}} = -2a^{1/2}\chi'(a) \tag{22}$$

where $\mathrm{Re}_{\bar{x}} = \frac{\overline{u_e}(\bar{x})\bar{x}}{\upsilon_f}$is the local Reynolds number.

5. MATLAB BVP5C computation, validation, results and discussion

Simulation of the transformed Eqns. 15–18 subject to the boundary conditions (19)–(20) are found with the help of Matlab buit in function bvp5c. MATLAB bvp5c solver is a superior algorithm to the more customary bvp4c solver, and directly controls the true error in the calculation, while bvp4c controls it only indirectly. At more stringent error tolerances, this difference between the solvers is not as apparent since Shampine-Kierzenka enhancement is employed which is absent in MATLAB bvp4c. bvp5c is a finite difference code that implements the four-stage Lobatto IIIa formula which is a collocation formula and the collocation polynomial provides a C [1]-continuous solution that is fifth-order accurate uniformly in [a,b]. The formula is implemented as an implicit Runge-Kutta formula. bvp5c does not utilize analytical condensation which is present in bvp4c. Unlike bvp4c which handles unknown parameters directly, bvp5c augments the system with trivial differential equations for the unknown parameters. For robustness the new solver is based on control of a residual. The residual is scaled so that it has the same order of convergence as the true error. For a large class of methods,

Table 1
Thermophysical properties of nanoparticles.

Materials	ρ $\left(kg/m^3\right)$	C_p $\left(J/kgK\right)$	K $\left(W/mK\right)$	$\alpha \times 10^{-5}$ $\left(m^2/s\right)$	σ $\left(S/m\right)$
Water (H_2O) at 17 °C	997.1	4179	0.613	1.43	5.5×10^{-6}
Copper oxide (CuO)	6500	535.6	20	0.57	5.96×10^{7}
Alumina (Al_2O_3)	3970	765	40	1.3	3.5×10^{7}
Titania (TiO_2)	4250	686.2	8.9538	0.31	2.38×10^{6}
Copper (Cu)	8933	385	401	11.7	5.8×10^{7}

bvp5c has been verified to confirm that if this scaled residual is less than a given tolerance, then asymptotically the true error is also less than the tolerance. Bvp5c interpolates the value and gradient at both ends of the subinterval and the value of y_{mid} at the midpoint. The following Russel-Christansen stepping formula is used in bvp5c:

$$Y_{MID} = Y_1 + \zeta\left[\frac{17}{192}K_1 + \frac{40+15\sqrt{5}}{192}K_2 + \frac{40-15\sqrt{5}}{192}K_3 - \frac{1}{192}K_4\right] \tag{23}$$

Here Y_1 is the initial guess and K_1, K_2, K_3, K_4 are the approximations with a stepping distance of ζ. The algorithm is very efficient, unconditionally stable and produces excellent accuracy with fast compilation times making it ideal for axisymmetric boundary layer multi-physical nanofluid magnetic bioconvection simulations, as reported here.

Four different metallic/metallic oxide-aqueous nanofluids, namely *Cu*-water, Al_2O_3-water, *CuO*-water and TiO_2-water nanofluids are investigated. Thermophysical properties of the base fluid and nanoparticles are displayed in Table 1 [48,53]. The Prandtl number (*Pr*) is set at 6.8 and the volume fraction of nanoparticles (Φ) is assumed in the range of $0 \leq \Phi \leq 0.2$. Comparisons with Chen and Smith [54] for regular Newtonian fluid ($\Phi = 0$) is shown in Table 2. Note that the present results are in favourable agreement. We also compare (Tables 2–5) the MATLAB bvp5c computational results with Grosan and Pop [55] (setting $n = 2m - 1$ in Ref. [55], allows for a comparison with the reduced present model given in Ref. [55]) and admirable agreement is obtained.

Profiles of dimensionless velocity $f'(\eta)$, temperature $\theta(\eta)$, nanoparticle volume fraction (nano-particle species concentration) $\varphi(\eta)$and motile micro-organism number density $\chi(\eta)$ for regular viscous fluid in the absence of nano-particles (i.e. $\Phi = 0$) are depicted in Fig. 2. Notice that all of the profiles obey free stream boundary conditions; velocity profile ascends monotonically and asymptotically tends to the free stream value; temperature, nanoparticle *concentration* and micro-organism density number profiles are also asymptotic at infinity but follow monotonic decays from the needle surface into the free stream. All profiles clearly indicate that the invicid boundary criteria is adequately large in the numerical solution.

Fig. 3(a–d) show the impact of different nanoparticles ($CuAl_2O_3CuO$, TiO_2) on dimensionless velocity, temperature, nanoparticle volume fraction and density of motile micro-organism number. Fig. 3(a) demonstrations that the velocity is highest for *Cu*and gradually decreases for $CuO, TiO_2$and is a minimum for Al_2O_3. The impact of nanoparticle material properties is simulated via the expressions A_0, A_1 and A_2, as defined in Eqn. (21) all of which are functions of the nanoparticle volume fraction, *Φ, which measures the percentage of doping of the base fluid (water)*. However in the Tiwari-Das model this volume fraction does not simulate the species diffusion of the nanoparticles (φ) for which a supplementary equation (17) is used. However it is to be noted that the present formulation is distinct from the Buongiorno two-component model since the nanoparticle concentration boundary layer equation does not feature Brownian motion or thermophoretic body force effects. Although numerous studies have utilized the Buongiorno model [56], there is no general consensus as yet to which mechanisms exactly contribute to enhanced thermal conductivity in nanofluids, as noted by Minkowycz [57]. The area if one of active exploration. Rana and Bég [58] have investigated a multiplicity of different effective thermal conductivity and viscosity models observing that these different formulations which concur more closely with the Twari-Das formulation as compared with the Buongiorno model, justifying the adoption of the latter in the present study. The presence of A_0 *and* A_1 parameters in the momentum boundary layer Eqn. (15) clearly modifies the momentum diffusion in the nanofluid bioconvection regime external to the needle. This in turn modifies the thermal diffusion in the nanofluid. Cooper which possesses the highest thermal conductivity is clearly observed to induce strong acceleration and titanium dioxide which possesses the lowest thermal conductivity produces deceleration. Nanoparticle properties therefore evidently impact on the momentum boundary layer thickness and in this regard thinner boundary layer structure is produced for copper whereas a thicker boundary layer is obtained for the other metallic oxide nanoparticles (Al_2O_3CuO, TiO_2) for which the oxygen content may contribute to a reduction in thermal conductivities. However as noted by Kuharat and Bég [59], thermal conductivity of copper does not always guarantee enhanced heating in nanofluid boundary layers in particular in forced convection flows (as studied here) which deviate from natural convection flows and produce different temperature distributions. This is confirmed in Fig. 3(b) where a marginally higher temperature is computed for Al_2O_3-water nanofluid, rather than copper-water nanofluid. TiO_2-water nanofluid also achieves a slightly higher temperature than either *Cu or CuO* water nanofluids, although it is exceeded by Al_2O_3-water nanofluid. Similarly higher nanoparticle concentration and motile micro-organism number density are attained with Al_2O_3, then TiO_2, CuO and finally the lowest value for *Cu*nanoparticles. This behaviour also agrees with the result reported in Ref. [55] although they did not consider magnetic nanofluids. Therefor maximum thermal boundary layer thickness, nanoparticle concentration boundary layer thickness and motile microorganism species boundary layer thickness are obtained consistently for the Al_2O_3 nanoparticles whereas the thinnest boundary layers correspond to *Cu* nanoparticles.

Table 2
Values of $-\theta'(a)$ for.$\Phi = 0$, $\Pr = 0.733$

a	$m = 0$				$m = 0.5$			
	$n = 0$		$n = 1$		$n = 0$		$n = 1$	
	Grosan and Pop [55]	Current work	Grosan and Pop [55]	Current work	Grosan and Pop [55]	Current work	Grosan and Pop [55]	Current work
0.1	2.441675 (2.434)	2.44175	2.920733 (2.920)	2.92362	2.516082 (2.505)	251464	3.027603 (3.026)	3.027603
0.01	16.306544	16.30767	18.704361	18.70573	16.535072	16.53619	19.069678	19.07110
0.001	120.55034	120.55072	134.17011	134.19841	121.51686	134.19841	135.67860	135.68944

( )values reported by Chen and Smith [54].

Table 3
Values of $f''(a)$for.$\Phi = n = 0,\ \mathrm{Pr} = 7$

a	$m = 0$			$m = 0.5$		
	Chen and Smith [54]	Grosan and Pop [55]	Current work	Chen and Smith [54]	Grosan and Pop [55]	Current work
0.1	1.28881	1.289074	1.28911	1.72178	1.721998	1.72186
0.01	8.49244	8.492173	8.49568	10.35056	10.35056	10.35292
0.001	62.16372	62.161171	62.16975	71.66594	71.667683	71.68430

Table 4
Values of $f''(a)$for.$m = n = 0,\ \mathrm{Pr} = 7$

Φ	a	Cu		Al_2O_3	
		Grosan and Pop [55]	Current work	Grosan and Pop [54]	Current work
0.05	0.1	1.347208	1.34916	1.293086	1.29202
	0.01	8.771680	8.77893	8.509033	8.50718
	0.001	63.884384	63.884384	62.544689	62.55452
0.1	0.1	1.382008	1.38524	1.288703	1.28814
	0.01	8.935933	8.93969	8.491924	8.49250
	0.001	64.653616	64.65473	62.373393	62.37810
0.2	0.1	1.404136	1.40624	1.266109	1.26688
	0.01	9.041011	9.04633	8.378166	8.37662
	0.001	65.235057	65.23006	61.516511	61.51942

Table 5
Values of $-\theta'(a)$ **for.**$m = n = 0,\ \mathrm{Pr} = 7$

Φ	a	Cu		Al_2O_3	
		Grosan and Pop [55]	Current work	Grosan and Pop [55]	Current work
0	0.1	3.770504	3.77048	3.770504	3.77048
	0.01	22.738762	22.74175	22.738762	22.74175
	0.001	156.137817	156.16709	156.137817	156.16709
0.05	0.1	3.682009	3.68355	3.652075	3.65385
	0.01	22.284916	22.28979	22.183096	22.18888
	0.001	153.570113	153.59936	153.157168	153.18582
0.1	0.1	3.586544	3.58741	3.538902	3.53985
	0.01	21.816182	21.81981	21.653419	21.65669
	0.001	150.977665	151.02182	150.314106	150.34170
0.2	0.1	3.389762	3.38987	3.325065	3.32597
	0.01	20.877668	20.87932	20.654662	20.65714
	0.001	145.860889	145.89365	144.934874	144.96030

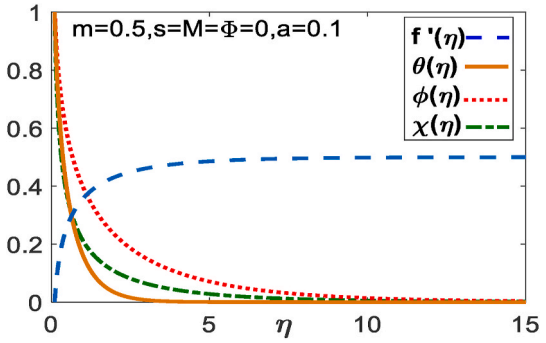

Fig. 2. Sample of$f'(\eta)$, $\theta(\eta)$, $\varphi(\eta)$and $\chi(\eta)$for regular viscous fluid.

Fig. 4(a–d) depict the effects of different *Cu* nanoparticle volume fraction (Φ) and the needle sizes (a) on transport characteristics. According to physical point of view, with an increase in nanoparticle volume fraction, both the viscosity and thermal conductivity of the nanofluid are enhanced (due to greater percentage doping), as per the Tiwari-Das formulations given earlier. With the increase of the volume fraction both the velocity and temperature increase, indicating that the flow is strongly enhanced and therefore that

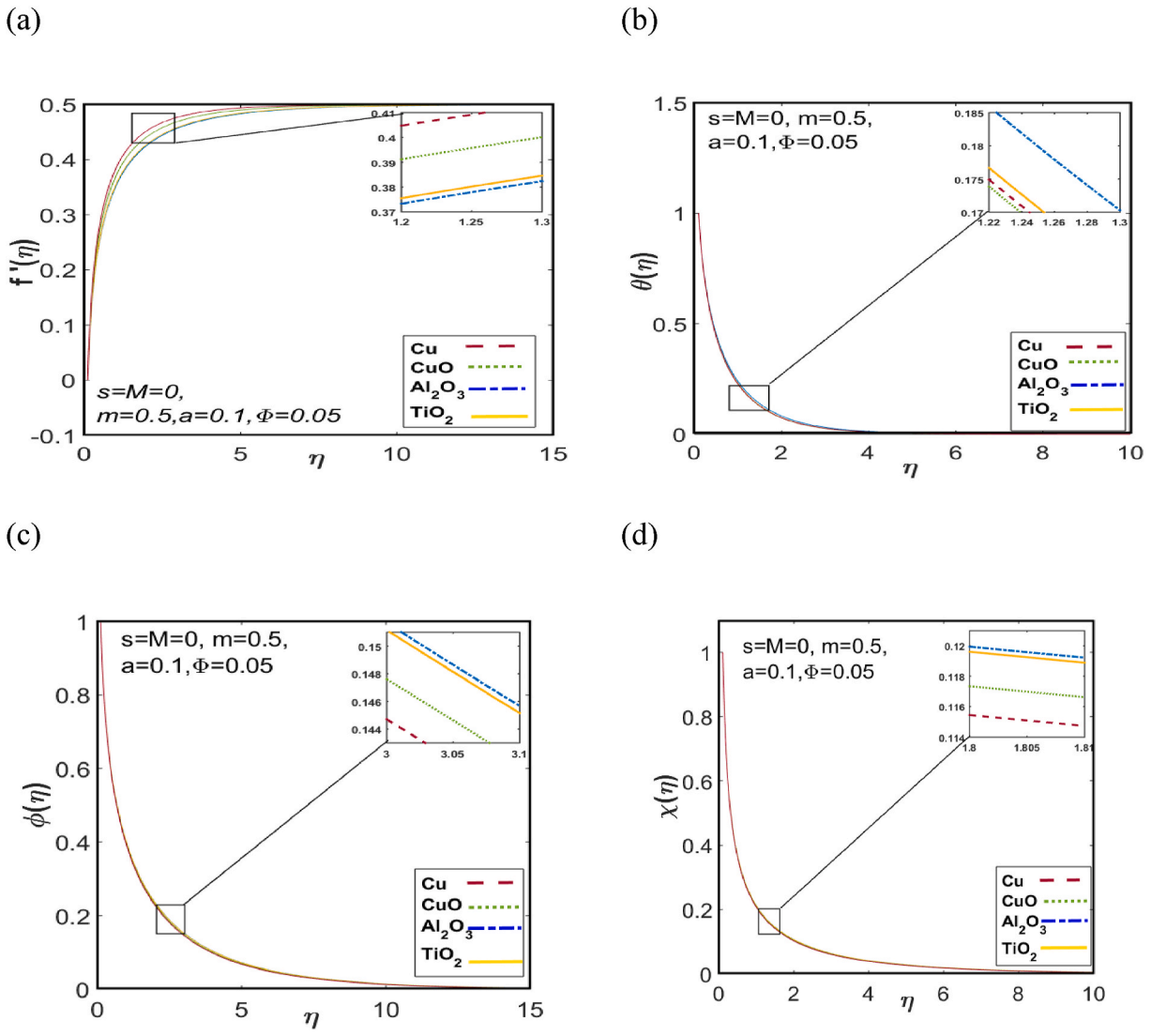

Fig. 3. Effects of various nanoparticles on $f'(\eta)$, $\theta(\eta)$, $\varphi(\eta)$and $\chi(\eta)$.

velocity boundary layer thickness is lessen. Energy (thermal) boundary layer thickness is however increased (Fig. 4(a&b)). It is also evident that velocity rises but temperature reduces with increases of needle size. The momentum development is enhanced with longer needles i.e. *progressively larger contact area* of the needle surface which assists in momentum diffusion, enhances the flow and decrease the momentum boundary layer thickness. Conversely the elevation in momentum diffusion rate inhibits the thermal diffusion which induces cooling of the boundary layer and a reduction in thermal boundary layer thickness. These patterns of behaviour concur with ref. [56]. No substantial modification in nano-particle species concentration or micro-organism density number is induced with a change in nano-particle volume fraction. Increasing needle size however does cause a marked reduction in both nanoparticle concentration and motile micro-organism density number since a greater space has to be occupied by the same quantity of nanoparticles and micro-organisms with larger dimensions of the needle (axisymmetric boundary layer) and there is corresponding decrease in boundary layer thicknesses (Fig. 4(c&d)).

Fig. 5(a&b) explains the effects of the magnetic field parameter (M) on velocity and temperature fields. The magnetic field is imposed radially, and this produces a Lorentzian drag force which significantly inhibits the flow i.e. reduces velocity magnitudes. The maximum velocity is therefore computed with $M = 0$ (no magnetic field) whereas the flow is all but eliminated at very high magnetic field ($M = 50$). The supplementary work exhausted in dragging the boundary layer flow in contradiction of the action of the magnetic field is dissipated as heat i.e. thermal energy. This elevates the temperatures in the boundary layer (Fig. 5(b)) and also enhances thermal boundary layer thickness. The implication is that with magnetic field presence, enhanced control of the boundary layer regime is achieved, which is not possible for non-magnetic nanofluids. No significant alteration in nano-particle concentration or micro-organism distribution is generated and therefore these figures are omitted. It is further of note that to properly invoke magnetic

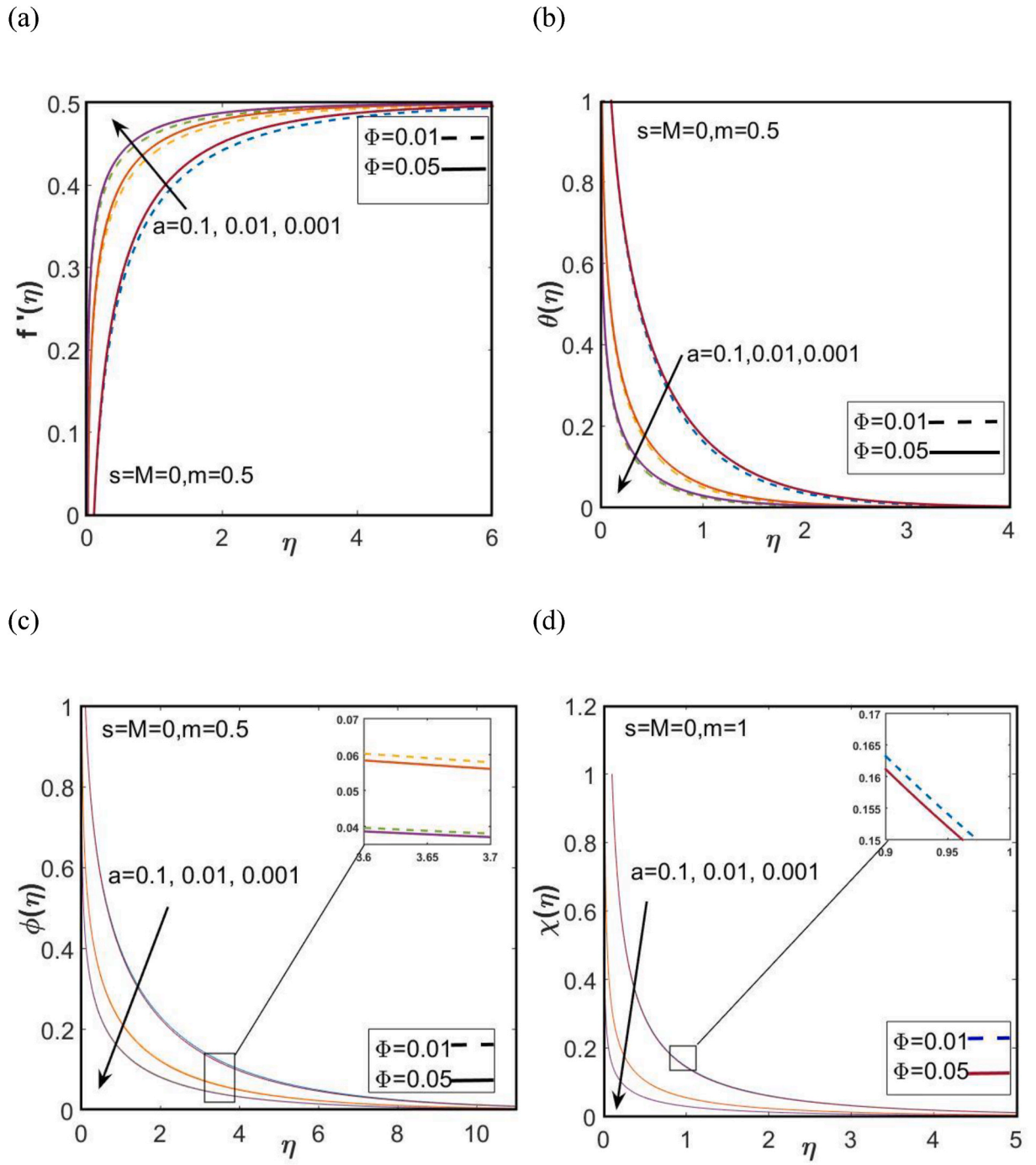

Fig. 4. Effects of needle size and *Cu*nanoparticles volume fractions on $f'(\eta)$, $\theta(\eta)$, $\varphi(\eta)$and $\chi(\eta)$.

effects on the micro-organisms, a magneto-tactic bioconvection model is required which may be addressed in future studies.

Fig. 6(a–c) visualize the effects of thermal power-law index parameter (m) and Stefan blowing parameter (s) on the dimensionless velocity, concentration and density of motile microorganism. The three different cases of suction ($s < 0$), injection ($s > 0$) and solid needle surface ($s = 0$) are analyzed. Fig. 6(a) reveals that velocity increases as m increases for both the permeable and solid needle designs. Momentum boundary layer thickness is therefore higher with greater non-isothermal effect. However, velocity is reduced for both isothermal ($m = 0$) and non-isothermal ($m = 1$) needle scenarios as the blowing parameter rises. The trends for nano-particle concentration (Fig. 6(b)) and motile micro-organism density number (Fig. 6(c)) are the opposite to those computed for the velocity for both isothermal and non-isothermal needles. Therefore, while the magnetic field has no tangible impact on nano-particle and

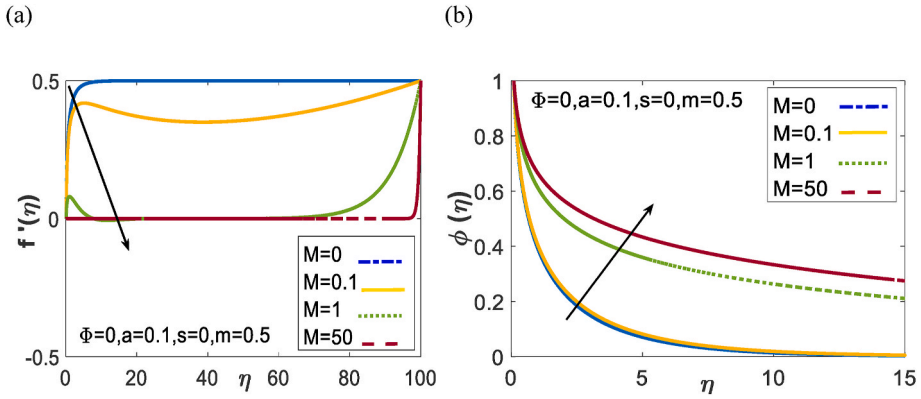

Fig. 5. Effect of magnetic field parameter (M) on $f^{'}(\eta)$ and $\theta(\eta)$for regular viscous fluid.

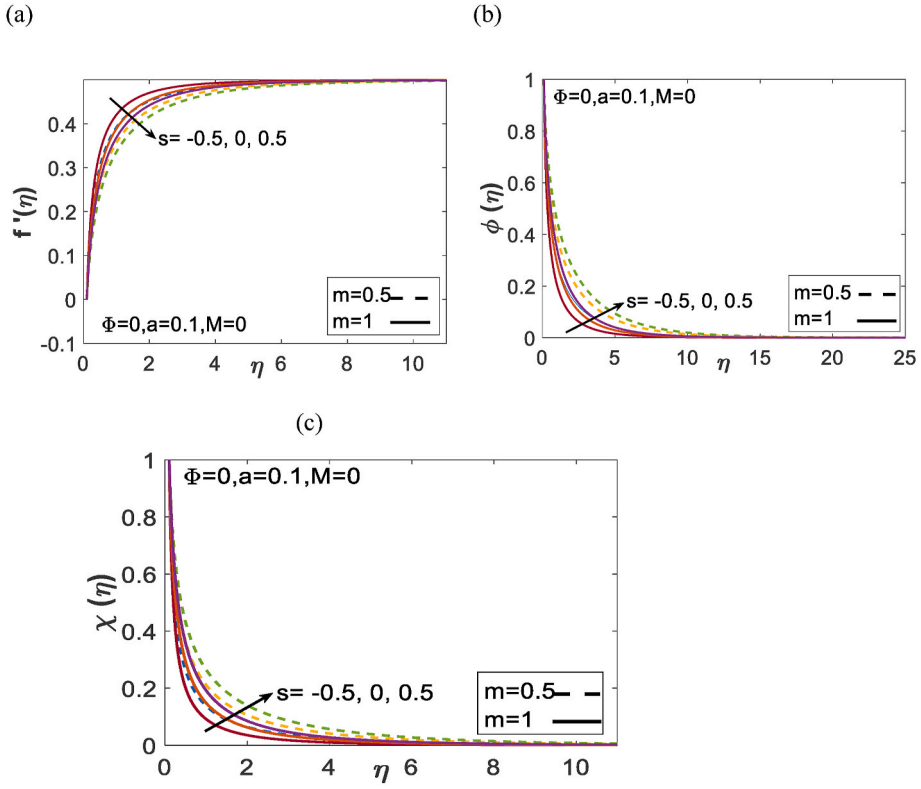

Fig. 6. The effect of s and m on $f^{'}(\eta)$, $\varphi(\eta)$, and $\chi(\eta)$for *CuO* nanoparticles.

micro-organism distributions, they are strongly affected by wall conditions (blowing or suction) and also non-isothermal effects and this is particularly important in transdermal pharmaceutical delivery systems as noted in Refs. [60,61].

We now focus our attention to scrutinize the effects *CuO* and TiO_2 nanoparticles on the wall gradient physical quantities. Tables 6 and 7 show the variation of the values of the local skin friction coefficient$f''(a)$, the local Nusselt number $-\theta^{'}(a)$, local Sherwood number $-\varphi^{'}(a)$and the local wall motile microorganism number $-\chi^{'}(a)$ for each of the four metallic nanofluids considered. All of the physical quantities decrease (increase) with an increase (decrease) in the Stefan blowing (index) parameter. The skin friction coefficient, rate of heat transfer, nanoparticle species mass transfer rate and motile microorganism density number gradient are highest for the suction case $s < 0$ (since this causes greater adhesion of the nanofluid to the needle surface and constraints transport to the surface rather than away from it) and lowest for injection cases > 0. For a particular needle size, skin friction and heat transfer rates for *CuO* water nanofluid are higher than that of TiO_2 water nanofluid. Finally, it is found that with greater needle sizes, skin friction coefficient, rate of heat transfer, nanoparticle species mass transfer rate and motile microorganism density number gradient consistently decrease.

Table 6
Physical quantities table of *CuO* for. $\Phi = 0.05, \mathrm{Pr} = 6.8, Sc = Sb = Pe = 1$

s	m	M	a	$f''(a)$	$-\theta'(a)$	$-\varphi'(a)$	$-\chi'(a)$
-0.5	0	0	0.1	3.15632	17.69760	5.91942	12.03342
0				2.20950	3.92672	4.27430	8.26126
0.5				1.75205	0.68573	3.46880	6.38351
0	0.5	0	0.1	2.35037	4.74437	4.41324	8.50774
	1			2.48557	5.41758	4.55468	8.75723
0	0	0.1	0.1	2.20770	3.92700	4.27435	8.26134
		1		2.03963	3.95349	4.27866	8.26853
		10		0.02929	4.31836	4.33880	8.36885
0	0	0	0.1	2.20950	3.92672	4.27430	8.26126
			0.01	11.12187	18.61627	21.22891	47.69737
			0.001	74.06730	123.94042	141.66896	357.76023

Table 7
Physical quantities table of TiO_2 for. $\Phi = 0.05, \mathrm{Pr} = 6.8, Sc = Sb = Pe = 1$

s	m	M	a	$f''(a)$	$-\theta'(a)$	$-\varphi'(a)$	$-\chi'(a)$
	0	0	0.1	3.06030	17.81470	5.92096	12.03619
-0.5							
0				2.20611	3.92440	4.27439	8.26142
0.5				1.78682	0.66835	3.46829	6.38271
0	0.5	0	0.1	2.33484	4.74526	4.41294	8.50716
	1			2.45884	5.41714	4.55329	8.75468
0	0	0.1	0.1	2.20432	3.92468	4.27444	8.26149
		1		2.03655	3.95131	4.27874	8.26867
		10		0.02928	4.31820	4.33881	8.36885
0	0	0	0.1	2.20611	3.92440	4.27439	8.26142
			0.01	11.09850	18.59956	21.22980	47.69886
			0.001	73.92119	123.81916	141.67431	357.76952

The thinnest needle produces the highest skin friction coefficient, rate of heat transfer, mass transfer and microorganism transfer rate. Therefore transport characteristics may be effectively manipulated with modification in the needle dimensions, although of course there is a critical upper limit to the sizes possible owing to medical requirements.

6. Conclusions

A new mathematical model for two-dimensional steady-state magnetohydrodynamic (MHD) forced bioconvection nanofluid flow along a stationary porous needle is presented. A Stefan-blowing condition is applied at the surface (wall) of the needle. The model provides a simulation of transdermal hypodermic needle fluid dynamics utilizing nanoparticles and biocompatible micro-organisms. A Tiwari-Das nanoscale model is adopted to investigate percentage doping of copper, copper oxide, aluminium oxide and titanium dioxide metallic nanoparticles dispersed in an aqueous base fluid. The governing equations are reduced to a similarity equations before being solving numerically. Following conclusions can be drawn.

(i) All physical quantities decrease with an increase in blowing parameter.
(ii) All physical quantities are highest for the suction case $s < 0$ and lowest for the injection cases > 0.
(iii) All physical quantities increase with an increase of non-isothermal power law index.
(iv) With an increase in magnetic field, skin friction coefficient is suppressed (strong deceleration) while the local Nusselt number, local Sherwood number, and the local wall motile microorganism density number increase. However, with stronger magnetic field effect, the nano-particle and micro-organisms density number functions are not influenced tangibly within the body of the nanofluid.
(v) Increasing power-law parameter accelerates the flow for both the permeable and solid needle designs.
(vi) For a specific needle size, skin friction and heat transfer rates for *CuO* water nanofluid are higher than that of TiO_2 water nanofluid.
(vii) With larger needle sizes, all physical quantities are reduced.

It can be concluded that, shear stress is highest for *Cu*-water and lowest for Al_2O_3-water, heat transfer rate is highest for Al_2O_3-water and lowest for TiO_2-water, mass and microorganism transfer rates are highest for Al_2O_3-water and lowest for Cu-water nanofluid. All

physical quantities are depleted in magnitude with increasing needle size. The problem considered here, relates with the applications to various transdermal delivery and biomedical electromagnetic treatments. This is an important area currently being deployed widely during the corona virus pandemic and demonstrates much greater safety than conventional transdermal delivery. These techniques feature multiple physical (electromagnetic, nanoscale, thermal and hydrodynamic slip) effecs and as such a robust analysis should feature all these characteristics. Biomagnetic thermal therapy in particular is a key clinical application which has become increasingly popular during the devastating worldwide covid 19 pandemic of 2020. Further details are given below in Refs. [62–64]. The leading biomagnetic researcher in the world, *Professor Dr. Hermann Berg of the Bioelectrochemistry Laboratory, Jena, Germany,* [65] has emphasized the potential of biomagnetic nano needle therapy as early as 2000. He has shown that currently, DC electrotherapy, pulse electrochemotherapy, and pulse electrogenetherapy are used widely and successfully to treat tumors. However, needle electrodes have to be inserted into the tumor region for pulse applications (about electrical field strength < 2 kV/cm). Only for skin carcinoma are caliper electrodes placed directly outside on the skin. External electromagnetic fields (magnetic field intensity > 5 mT) generated by Helmholtz coils or solenoids offer a novel non-invasive cancerostatic possibility. Nevertheless, this adjuvant non-invasive therapy in synergistic combination with cancerostatic agents, hyperthermia, and photodynamics has great promise for transdermal treatments in the coming decades. The present model constitutes a first simulation in this regard, and moreover provides a good solid benchmark for generalization to three dimensional (axisymmetric) computational fluid dynamics simulations using ANSYS FLUENT finite volume code, COMSOL, OPENFOAM and ADINA finite element commercial solvers. In this light the current problem can also be extended further considering thermal radiation, chemical attraction, for *unsteady flow* and also non-Newtonian fluid characteristics in addition to different micro-organism taxes e.g. *magneto-taxis* with 3-dimensional numerical visualization and wefforts in this regard are currently under way.

Author statement

The authors would like to thank the reviewers for their valuable comments and suggestions. The paper has been revised in the light of these comments. We believe that we have answered and resolved every query posed by the **reviewers** carefully and adequately. We feel the article is now worthy of the standard of the journal and anticipate a positive response. In the revised manuscript the corrected/ inserted parts are shown in coloured letters and highlights. Please note we have slightly modified the title of the paper to better reflect the subject content.

CRediT authorship contribution statement

O. Anwar Beg: Writing - review & editing, Investigation. **F.T. Zohra:** Writing - original draft, preparation, Software, Visualization, Validation. **M.J. Uddin:** Conceptualization, Methodology, Investigation. **A.I.M. Ismail:** Writing - original draft, preparation, Supervision. **Saratha Sathasivam:** Writing - review & editing, Software, Data curation.

Declaration of competing interest

The authors do not have any conflict of interest.

Acknowledgements

Professor O. Anwar Bég would like to express his gratitude to *Professor Sheila Pankhurst*, formerly Dean of the School of Science, Engineering and Environment (SEE) for her sustained encouragement with novel biomedical fluid dynamics research. He also wishes to express his gratitude to *Miss Maria Baranquilla* of Colombia, for some recent excellent discussions on bioelectromagnetic therapy for feet relaxation and stimulative treatment which aided in identifying new applications of the work. The authors acknowledge financial support from Universiti Sains Malaysia, RUI Grant (1001/PMATHS/8011131). All the authors also acknowledge most gratefully the comments of the reviewers which have improved the work.

References

[1] F.T. Zohra, M.J. Uddin, A.I.M. Ismail, Magnetohydrodynamic bio-nanoconvective Navier slip flow of micropolar fluid in a stretchable horizontal channel, Heat Tran. Asian Res. 48 (8) (2019) 3636–3656.
[2] K.U. Rehman, Q.M. Al-Mdallal, M.Y. Malik, Symmetry analysis on thermally magnetized fluid flow regime with heat source/sink, Case Stud. Therm. Eng. (2019) 14.
[3] K.U. Rehman, I. Shahzadi, M.Y. Malik, Q.M. Al-Mdallal, M. Zahri, On heat transfer in the presence of nano-sized particles suspended in a magnetized rotatory flow field, Case Stud. Therm. Eng. 14 (2019).
[4] A.M. Rashad, M.M. Rashidi, G. Lorenzini, S.E. Ahmed, A.M. Aly, Magnetic field and internal heat generation effects on the free convection in a rectangular cavity filled with a porous medium saturated with Cu–water nanofluid, Int. J. Heat Mass Tran. 104 (2017) 878–889.
[5] O. Anwar Bég, A. Sohail, T.A. Bég, A. Kadir, B-spline collocation simulation of nonlinear transient magnetic nano-bio-tribological squeeze film flow, J. Mech. Med. Biol. 18 (2018) 20, https://doi.org/10.1142/S0219519418500070, 1850007.1- 181850007.20.
[6] K.L. Hsiao, Micropolar nanofluid flow with MHD and viscous dissipation effects towards a stretching sheet with multimedia feature, Int. J. Heat Mass Tran. 112 (2017) 983–990, https://doi.org/10.1016/J.IJHEATMASSTRANSFER.2017.05.042.
[7] A. López, G. Ibáñez, J. Pantoja, J. Moreira, O. Lastres, Entropy generation analysis of MHD nanofluid flow in a porous vertical microchannel with nonlinear thermal radiation, slip flow and convective-radiative boundary conditions, Int. J. Heat Mass Tran. 107 (2017) 982–994, https://doi.org/10.1016/J.IJHEATMASSTRANSFER.2016.10.126.

[8] A. Raees, H. Xu, S.J. Liao, Unsteady mixed nano-bioconvection flow in a horizontal channel with its upper plate expanding or contracting, Int. J. Heat Mass Tran. 86 (2015) 174–182, https://doi.org/10.1016/J.IJHEATMASSTRANSFER.2015.03.003.

[9] T. Burghelea, E. Segre, I. Bar-Joseph, A. Groisman, V. Steinberg, Chaotic flow and efficient mixing in a microchannel with a polymer solution, Phys. Rev. 69 (2014) 66305, https://doi.org/10.1103/PhysRevE.69.066305.

[10] T.L. Stewart, H.S. Fogler, Biomass plug development and propagation in porous media, Biotechnol. Bioeng. 72 (2001) 353–363. http://www.ncbi.nlm.nih.gov/pubmed/11135206. (Accessed 9 January 2018).

[11] K. Li, S. Liu, X. Liu, An overview of algae bioethanol production, Int. J. Energy Res. 38 (2007) 965–977, https://doi.org/10.1002/er.3164.

[12] Y. Chisti, Biodiesel from microalgae, Biotechnol. Adv. 25 (2007) 294–306, https://doi.org/10.1016/J.BIOTECHADV.2007.02.001.

[13] E. Molina, J. Fernández, F.G. Acién, Y. Chisti, Tubular photobioreactor design for algal cultures, J. Biotechnol. 92 (2001) 113–131, https://doi.org/10.1016/S0168-1656(01)00353-4.

[14] E. Le, C. Park, S. Hiibel, Investigation of the effect of growth from low to high biomass concentration inside a photobioreactor on hydrodynamic properties of scenedesmus obliquus, ASME Journal of Energy Resources Technology 134 (2012) 11801, https://doi.org/10.1115/1.4005245.

[15] D. Mansoury, F. Ilami Doshmanziari, S. Rezaie, M.M. Rashidi, Effect of Al 2 O 3/water nanofluid on performance of parallel flow heat exchangers: an experimental approach, J. Therm. Anal. Calorim. 135 (2019) 625–643.

[16] R. Mohebbi, M.M. Rashidi, Numerical simulation of natural convection heat transfer of a nanofluid in an L-shaped enclosure with a heating obstacle, J. Taiwan Inst. Chem. Eng. 72 (2017) 70–84.

[17] A. Sohail, Z. Li (Eds.), Computational Approaches in Biomedical Nano-Engineering, vol. 5, Wiley-CVH, China, 2018, pp. 100–130.

[18] M.J. Uddin, Y. Alginahi, O. Anwar Bég, M.N. Kabir, Numerical solutions for gyrotactic bioconvection in nanofluid-saturated porous media with Stefan blowing and multiple slip effects, Comput. Math. Appl. 72 (2016) 2562–2581, https://doi.org/10.1016/J.CAMWA.2016.09.018.

[19] N. Acharya, K. Das, P.K. Kundu, Framing the effects of solar radiation on magneto-hydrodynamics bioconvection nanofluid flow in presence of gyrotactic microorganisms, J. Mol. Liq. 222 (2016) 28–37, https://doi.org/10.1016/J.MOLLIQ.2016.07.023.

[20] J.J. Li, H. Xu, A. Raees, Q.K. Zhao, Unsteady mixed bioconvection flow of a nanofluid between two contracting or expanding rotating discs, Z. Naturforsch. (2016) 261–272, https://doi.org/10.1515/zna-2015-0518, 0.

[21] N. Begum, S. Siddiqa, M. Sulaiman, S. Islam, M.A. Hossain, R.S.R. Gorla, Numerical solutions for gyrotactic bioconvection of dusty nanofluid along a vertical isothermal surface, Int. J. Heat Mass Tran. 113 (2017) 229–236.

[22] S. Mosayebidorcheh, M.A. Tahavorim, T. Mosayebidorcheh, D.D. Ganji, Analysis of nano-bioconvection flow containing both nanoparticles and gyrotactic microorganisms in a horizontal channel using modified least square method (MLSM), J. Mol. Liq. 227 (2017) 356–365, https://doi.org/10.1016/j.molliq.2016.12.039.

[23] S. Farooq, T. Hayat, A. Alsaedi, B. Ahmad, Numerically framing the features of second order velocity slip in mixed convective flow of Sisko nanomaterial considering gyrotactic microorganisms, Int. J. Heat Mass Tran. 112 (2017) 521–532, https://doi.org/10.1016/J.IJHEATMASSTRANSFER.2017.05.005.

[24] U. Ali, K.U. Rehman, A.S. Alshomrani, M.Y. Malik, Thermal and concentration aspects in Carreau viscosity model via wedge, Case Stud. Therm. Eng. 12 (2018) 126–133.

[25] K.U. Rehman, A.S. Alshomrani, M.Y. Malik, Carreau fluid flow in a thermally stratified medium with heat generation/absorption effects, Case Stud. Therm. Eng. 12 (2018) 16–25.

[26] U. Ali, K.U. Rehman, M.Y. Malik, I. Zehra, Thermal aspects of Carreau fluid around a wedge, Case Stud. Therm. Eng. 12 (2018) 462–469.

[27] K.U. Rehman, N.U. Saba, M.Y. Malik, A.A. Malik, Encountering heat and mass transfer mechanisms simultaneously in Powell-Erying fluid through Lie symmetry approach, Case Stud. Therm. Eng. 10 (2017) 541–549.

[28] K.U. Rehman, A.S. Alshomrani, M.Y. Malik, I. Zehra, M. Naseer, Thermo-physical aspects in tangent hyperbolic fluid flow regime: a short communication, Case Stud. Therm. Eng. 12 (2018) 203–212.

[29] F.T. Zohra, M.J. Uddin, A.I.M. Ismail, O. Anwar Bég, A. Kadir, Anisotropic slip magneto-bioconvection flow from a rotating cone to a nanofluid with Stefan blowing effects, Chin. J. Phys. 56 (1) (2018) 432–448, https://doi.org/10.1016/j.cjph.2017.08.031.

[30] C. Sulochana, G.P. Ashwinkumar, N. Sandeep, Joule heating effect on a continuously moving thin needle in MHD Sakiadis flow with thermophoresis and Brownian moment, The European Physical Journal Plus 132 (2017) 387, https://doi.org/10.1140/epjp/i2017-11633-3.

[31] F.C. Lai, C.Y. Choi, F.A. Kulacki, Coupled heat and mass transfer by natural convection from slender bodies of revolution in porous media, Int. Commun. Heat Mass Tran. 17 (1990) 609–620, https://doi.org/10.1016/0735-1933(90)90009-9.

[32] J.P. Narain, M.S. Uberoi, Combined forced and free-convection over thin needles, Int. J. Heat Mass Tran. 16 (1973) 1505–1512, https://doi.org/10.1016/0017-9310(73)90179-8.

[33] C.Y. Wang, Mixed convection on a vertical needle with heated tip, Phys. Fluid. Fluid Dynam. 2 (1990) 622–625, https://doi.org/10.1063/1.857709.

[34] C.Y. Ishak, R. Nazar, I. Pop, Boundary layer flow over a continuously moving thin needle in a parallel free stream, Chin. Phys. Lett. 24 (2007) 2895–2897, https://doi.org/10.1088/0256-307X/24/10/051.

[35] R. Trimbitas, T. Grosan, I. Pop, Mixed convection boundary layer flow along vertical thin needles in nanofluids, Int. J. Numer. Methods Heat Fluid Flow 24 (2014) 579–594, https://doi.org/10.1108/HFF-05-2012-0098.

[36] T. Hayat, M.I. Khan, M. Farooq, T. Yasmeen, A. Alsaedi, Water-carbon nanofluid flow with variable heat flux by a thin needle, J. Mol. Liq. 224 (2016) 786–791, https://doi.org/10.1016/J.MOLLIQ.2016.10.069.

[37] C. Sulochana, S.P. Samrat, N. Sandeep, Boundary layer analysis of an incessant moving needle in MHD radiative nanofluid with Joule heating, Int. J. Mech. Sci. 128–129 (2017) 326–331, https://doi.org/10.1016/J.IJMECSCI.2017.05.006.

[38] N.S. Akbar, A.B. Huda, M.B. Habib, D. Tripathi, Nanoparticles shape effects on peristaltic transport of nanofluids in presence of magnetohydrodynamics, Microsyst. Technol. 25 (2019) 283–294.

[39] N.S. Akbar, M.B. Habib, Peristaltic pumping with double diffusive natural convective nanofluid in a lopsided channel with accounting thermophoresis and Brownian Moment, Microsyst. Technol. 25 (2019) 1217–1226.

[40] N.S. Akbar, M. Shoaib, D. Tripathi, S. Bhushan, O. Anwar Bég, Analytical approach to entropy generation and heat transfer in CNT-nanofluid dynamics through a ciliated porous medium, Journal of Hydrodynamics, Ser. B. 30 (2) (2018) 296–306.

[41] N.S. Akbar, A.W. Butt, Ferromagnetic nano model study for the peristaltic flow in a plumb duct with permeable walls, Microsyst. Technol. 25 (2018) 1227–1234.

[42] N.S. Akbar, D. Tripathi, Z.H. Khan, O. Anwar Bég, Mathematical modelling of pressure-driven micropolar biological flow due to metachronal wave propulsion of beating cilia, Math. Biosci. 301 (2018) 121–128, https://doi.org/10.1016/j.mbs.2018.04.001.

[43] R. Ahmad, M. Mustafa, S. Hina, Buongiorno's model for fluid flow around a moving thin needle in a flowing nanofluid: a numerical study, Chin. J. Phys. 55 (2017) 1264–1274, https://doi.org/10.1016/J.CJPH.2017.07.004.

[44] M.I. Afridi, M. Qasim, Entropy generation and heat transfer in boundary layer flow over a thin needle moving in a parallel stream in the presence of nonlinear Rosseland radiation, Int. J. Therm. Sci. 123 (2018) 117–128, https://doi.org/10.1016/J.IJTHERMALSCI.2017.09.014.

[45] N.A. Amirsom, Mohammed Jashim Uddin, and Ahmad Izani md Ismail. MHD boundary layer bionanoconvective non-Newtonian flow past a needle with Stefan blowing, Heat Tran. Asian Res. 48 (2) (2019) 727–743.

[46] L.F. Shampine, J. Kierzenka, A BVP solver that controls residual and error, Numer. Anal. Ind. Appl. Math. 3 (1–2) (2008) 27–41.

[47] T. Fang, W. Jing, Flow, heat, and species transfer over a stretching plate considering coupled Stefan blowing effects from species transfer, Commun. Nonlinear Sci. Numer. Simulat. 19 (2014) 3086–3097, https://doi.org/10.1016/J.CNSNS.2014.02.009.

[48] H.F. Oztop, E. Abu-Nada, Numerical study of natural convection in partially heated rectangular enclosures filled with nanofluids, Int. J. Heat Fluid Flow 29 (2008) 1326–1336, https://doi.org/10.1016/J.IJHEATFLUIDFLOW.2008.04.009.

[49] K. Vajravelu, K.V. Prasad, J. Lee, C. Lee, I.V. Pop, R.A. Gorder, Convective heat transfer in the flow of viscous Ag–water and Cu–water nanofluids over a stretching surface, Int. J. Therm. Sci. 50 (2011) 843–851, https://doi.org/10.1016/J.IJTHERMALSCI.2011.01.008.

[50] M. Sheikholeslami, M. Hatami, D.D. Ganji, Analytical investigation of MHD nanofluid flow in a semi-porous channel, Powder Technol. 246 (2013) 327–336, https://doi.org/10.1016/J.POWTEC.2013.05.030.
[51] M.J. Uddin, M.N. Kabir, O. Anwar Bég, Computational investigation of Stefan blowing and multiple-slip effects on buoyancy-driven bioconvection nanofluid flow with microorganisms, Int. J. Heat Mass Tran. 95 (2016) 116–130, https://doi.org/10.1016/J.IJHEATMASSTRANSFER.2015.11.015.
[52] R. Seshadri, T.Y. Na, Group Invariance in Engineering Boundary Value Problems, Springer, New York, 1985, https://doi.org/10.1007/978-1-4612-5102-6.
[53] W.N. Mutuku, Ethylene glycol (EG)-based nanofluids as a coolant for automotive radiator, Asia Pac. J. Chem. Eng. 3 (2016) 1, https://doi.org/10.1186/s40540-016-0017-3.
[54] J.L.S. Chen, T.N. Smith, Forced convection heat transfer from non-isothermal thin needles, ASME Journal of Heat Transfer 100 (1978) 358, https://doi.org/10.1115/1.3450809.
[55] T. Grosan, I. Pop, Forced convection boundary layer flow past nonisothermal thin needles in nanofluids, ASME Journal of Heat Transfer 133 (2011) 54503, https://doi.org/10.1115/1.4003059.
[56] J. Buongiorno, Convective transport in nanofluids, ASME J Heat Transfer 128 (2006) 240–250.
[57] W.J. Minkowycz, E.M. Sparrow, Abraham, *Nanoparticle Heat Transfer And Fluid Flow* (Advances in Numerical Heat Transfer: Computational and Physical Processes in Mechanics and Thermal Sciences Book 4), CRC Press, 2016.
[58] P. Rana, O. Anwar Bég, Mixed convection flow along an inclined permeable plate: effect of magnetic field, nanolayer conductivity and nanoparticle diameter, Appl. Nanosci. 5 (2015) 569–581.
[59] S. Khurat, O. Anwar Bég, Computational fluid dynamics simulation of a nanofluid-based annular solar collector with different metallic nanoparticles, Heat and Mass Transfer Research Journal 3 (1) (2019) 1–23.
[60] S. Henry, D.V. Mc Allister, M.G. Allen, M.R. Prausnitz, Microfabricated micro- needles: a novel approach to transdermal drug delivery, J. Pharmaceut. Sci. 87 (1998) 922–925.
[61] W. Martanto, S.P. Davis, N.R. Holiday, J. Wang, H. Gill, Transdermal delivery of insulin using microneedles in vivo, Pharmaceut. Res. 21 (2004) 947–952.
[62] H. Berg, Bioelectric and biomagnetic methods for cancer research and therapy—a survey, Electromagn. Biol. Med. 24 (2005) 423–440.
[63] L. Zhang, In vivo skin-targeted gene delivery by pulsed electric fields, in: M. Jaroszeski, R. Heller, R. Gilbert (Eds.), Electrochemotherapy, Electrogenetherapy, and Transdermal Drug Delivery, Humana Press, Totowa, 2000.
[64] A. Liboff, et al., The charge and mass ICR signature in weak ELF bioelectromagnetic effects, in: J. Lin (Ed.), Advances in Electromagnetic Fields in Living Systems, Kluwer/Plenum, NY, 2003.
[65] H. Berg, Milestones of bioelectromagnetics: monographs and proceedings, Electromagn. Biol. Med. 25 (2004) 181–184.